polymers

MDPI

Article

Non-Isothermal Cold-Crystallization Behavior and Kinetics of Poly(L-Lactic Acid)/WS_2 Inorganic Nanotube Nanocomposites

Mohammed Naffakh [1,*], Carlos Marco [2] and Gary Ellis [2]

Received: 9 July 2015 ; Accepted: 22 October 2015 ; Published: 29 October 2015
Academic Editor: Patrick Ilg

[1] Escuela Técnica Superior de Ingenieros Industriales, Universidad Politécnica de Madrid (ETSII-UPM), José Gutiérrez Abascal 2, 28006 Madrid, Spain
[2] Instituto de Ciencia y Tecnología de Polímeros (ICTP-CSIC), Juan de la Cierva 3, 28006 Madrid, Spain; cmaroc@ictp.csic.es (C.M.); gary@ictp.csic.es (G.E.)
* Correspondence: mohammed.naffakh@upm.es; Tel.: +34-913-363-164; Fax: +34-913-363-007

Abstract: In order to accelerate the crystallization of poly(L-lactic acid) (PLLA) biopolymer and enhance its crystallizability, biocompatible and environmentally friendly tungsten disulphide inorganic nanotubes (INT-WS_2) were introduced into the polymer matrix. The non-isothermal cold-crystallization and subsequent melting behaviour of pure PLLA and PLLA/INT-WS_2 nanocomposites were investigated in detail by varying both the heating rate and INT-WS_2 loading. The kinetic parameters of the cold-crystallization process of PLLA chains under confined conditions, successfully described using Liu model, shows that the addition of INT-WS_2 significantly increased the crystallization rate and reduced the total cold-crystallinity of PLLA, while the crystallization mechanism and crystal structure of PLLA remained unchanged in spite of the INT-WS_2 loading. Similarly, the final crystallinity and melting behaviour of PLLA were controlled by both the incorporation INT-WS_2 and variation of the heating rate. The differential isoconversional method of Friedman was applied to estimate the dependence of the effective activation energy on the relative crystallinity and temperature for PLLA and PLLA/INT-WS_2. On the other hand, the double-melting peaks, mainly derived from melting-recrystallization-melting processes upon heating, and their dynamic behaviour is coherent with a remarkable nucleation-promoting effect of INT-WS_2 involved in accelerating the cold-crystallization of PLLA. These observations have considerable practical significance for the future sustainable, economic and effective technological utilisation of PLLA, as it will enable the development of novel melt-processable biopolymer nanocomposite materials.

Keywords: inorganic nanotubes; biopolymer; nanomaterials; crystallization kinetics; melting

1. Introduction

Poly(L-lactide acid) (PLLA) is a well-known thermoplastic considered among the family of environmentally friendly polymers that has attracted increasing attention in recent years because it can be produced from renewable resources, such as corn, and is non-toxic to the human body [1–3]. It exhibits multifunctional properties such as biodegradability (hydrolytic) and biocompatibility, good transparency, excellent tensile strength, and tensile modulus. Thus, PLLA offers great promise as one of the select few candidates for use in biomedical applications such as surgical sutures, bone fixation devices, and controlled drug-delivery systems. Moreover, due to its favorable biodegradability, good mechanical properties, and versatile fabrication processes, it has excellent potential for substitution of petroleum-based polymers [4–6]. Unfortunately, PLLA has several drawbacks, in terms of the processability and mechanical properties. The crystallization rate of PLLA is very slow, resulting in

the long processing cycle time and low production efficiency of products in the melt processing and molding. Therefore, the improvement of the thermal properties and crystallizability PLLA would be necessary in order to produce PLLA composites with desired performance [7].

In recent years, the incorporation of layered metal dichalcogenide (tungsten disulfide, WS_2 and molybdenum disulfide, MoS_2) nanophases in the polymer systems has become a field of recent interest as it opens opportunities for many new applications [8,9]. Since the discovery of such nanophases in 1992 and 1993 [10,11] many new inorganic nanotubes (INT) and inorganic fullerene-like (IF) nanoparticles have been synthesized from variety of compounds with layered (2D) nanostructures (e.g., transition metal disulfides: MoS_2, NbS_2, TaS_2, TiS_2, and ReS_2); transition metal oxides: Cs_2O, Tl_2O; halides: CdI_2; BN nanotubes, *etc.*). Diverse synthetic strategies have been developed or adapted for the synthesis of these nanostructures, including laser ablation, self-assembly, template synthesis, hydrothermal processing, metal–organic chemical vapor deposition (MOCVD), spray pyrolysis, microwave induced plasmas, gas–solid reactions and fluidized bed reactors) [12–15]. In the case of IF- and INT-WS2, careful investigation of the growth mechanism resulted in the synthesis of a pure phase, and the breakthrough development of a one-pot reaction, *i.e.*, via a sequence of reactions taking place in a single vertical reactor [16,17], paved the way to large-scale production for a broad range of applications. These nanotubes possess a highly perfect crystalline structure and consequently exhibit very desirable mechanical properties. They are ultra-strong impact-resistant materials with potential uses in personal protection (bullet-proof vests, helmets, *etc.*) and other safety equipment, car bumpers, high strength adhesives and binders, amongst others [18]. In addition to protective materials, WS_2 nanotubes can also be employed in nanoelectronics, fuel cells, ultra-filtration membranes, and catalysts [14,15]. Their optical properties allow various other applications in fields such as nanolithography or photocatalysis [19]. Equally important, the cytotoxicity of the INT-WS_2 was evaluated positively in comparison to standard environmental particulate matter, demonstrating much lower cytotoxicity than other nanoparticles, such as silica or carbon black [20]. Promising results have also been recently found with respect to the biocompatibility of INT(IF)-WS_2 with salivary gland cells [21]. With such excellent properties, and relatively simple and inexpensive fabrication, the incorporation of INT-WS_2 in polymer systems has become increasingly important [22–25].

In this regard, inorganic nanotubes (INT-WS_2) were well-dispersed into a PLLA matrix through simple melt blending, and the thermomechanical properties were investigated in detail with various techniques such as ultra-high field emission scanning microscopy (FE-SEM), time-resolved synchrotron X-ray, diffraction differential scanning calorimetry (DSC), thermogravimetric analysis (TGA) and dynamic mechanical analysis (DMA) [26]. The excellent dispersion of INT-WS_2 confirmed by FE-SEM lead to composites with substantially enhanced thermal and mechanical properties. However, to date the influence of the INT-WS_2 on the cold-crystallization behaviour of PLLA has not been investigated. The present research continues work in this field and focuses on the use of INT-WS_2 to improve the cold-crystallizability of PLLA. In this study, we analyzed the role of the INT-WS_2 concentration on the non-isothermal cold-crystallization and melting behaviour of PLLA polymer chains under confined conditions. This is because the knowledge of the cold-crystallization behaviour is valuable for the processing and use of PLLA.

2. Experimental Section

2.1. Materials and Processing

The biopolymer matrix was poly(L-lactic acid) (PLLA) purchased from Goodfellow Ltd. (density = 1.25 g/cm^3, $M_w \approx 1.5 \times 10^5$ g/mol, Cambridge, UK). Multiwall WS_2 nanotubes (INT-WS_2) with diameters of 30–150 nm and lengths of 1–20 μm were obtained from NanoMaterials Ltd (Yavne, Israel). Each mixture of PLLA and INT-WS_2 (0.1, 0.5 and 1.0 wt %) was dispersed in a small volume of ethanol and homogenized by mechanical stirring and bath ultrasonication for

approximately 10 min. Subsequently, the dispersion was partially dried in vacuum at 60 °C under a pressure of about 70 mbar for 24 h. Melt-mixing of the resulting dispersions was performed using a micro-extruder (Thermo-Haake Minilab system, Madison, WI, USA) operated at 190 °C and a rotor speed of 100 rpm for 10 min. This strategy yields finer dispersion, with INT-WS_2 almost fully debundled into individual tubes, which are randomly oriented in the PLLA matrix [26]. In no case was severe aggregation of nonmodified INT-WS_2 observed in the PLLA matrix despite the INTs loadings, indicating that the variation of INT-WS_2 contents from 0.1 to 1.0 wt % does not significantly affect the dispersion and distribution of INT-WS_2 in the polymer matrix.

2.2. Characterization Techniques

The morphology and structure of PLLA/INT-WS_2 nanocomposites were first characterized by ultra-high field-emission scanning microscopy (FE-SEM, SU8000, Hitachi Co., Tokyo, Japan) and wide angle X-ray scattering (WAXS, Desy-Hasylab, Hamburg, Germany) experiments using synchrotron radiation [26]. The processability and dispersion of INT-WS_2 was considered when evaluating thermal and mechanical response and performance of these new formulations in comparison with those previously reported in other PLLA nanocomposite systems. Successful dispersions of INT-WS_2 have been demonstrated by a remarkable improvement in the melt-crystallization processes and dynamic-mechanical properties of PLLA.In particular, it was found that 0.5 wt % loading led to the highest property improvements.

DSC cold-crystallization experiments were performed on a Perkin Elmer DSC7/Pyris differential scanning calorimeter (Perkin-Elmer España SL, Madrid, Spain), operating under nitrogen flow. Samples of 10 mg sealed in aluminum pans were initially held at 225 °C for 5 min, cooled to 40 °C at a rate of 40 °C/min and then reheated to 225 °C at a rate of 1, 2, 5, 10 and 20 °C/min, respectively. The melting temperature (T_m) and the cold-crystallization peak temperature (T_{cc}) were determined from the maximum of the melting endotherm and the minimum of the crystallization exotherm observed during the heating scan, respectively. The crystallinity (1-λ) was calculated as follows:

$$(1-\lambda) = \frac{\Delta H_c}{\Delta H_m^0} \quad (1)$$

where ΔH_c is the crystallization enthalpy and $\Delta H^0{}_m$ is the enthalpy of melting for perfect crystals: 93 J/g [27].

3. Results and Discussion

3.1. Non-Isothermal Cold-Crystallization Behavior

The crystallization of isotropic polymers by heating above the glass transition temperature (T_g) is denominated cold-crystallization. Unlike melt crystallization, in which the motion of polymer chains can be carried out entirely via molecular reptation [28], the polymer chains in the rubbery state complete the corresponding conformational rearrangements via cooperative segmental movements [29]. As a result, the crystal structure and morphology obtained from cold-crystallization may be expected to differ from that obtained by melt-crystallization. In addition, it well-known that the molecular motion of semicrystalline polymers above T_g involves discrete interaction between amorphous and crystalline regions. The formation and development of crystalline regions inevitably limits the motion of polymer chains in the amorphous region. This is especially important when the low heating rate is used. Thus, investigation of the cold-crystallization behaviour of amorphous samples contributes to further understanding of the kinetic behaviour of polymer chains under confined conditions.

PLLA manifests slow crystallization on cooling from the melt. It does not apparently crystallize if it is cooled at a rate of 20 °C/min or faster [26]. However, on subsequent heating after rapid cooling from the melt, the cold-crystallization phenomenon occurs. For the study of the

cold-crystallization process and the melting of non-isothermally cold-crystallized PLLA/INT-WS_2 nanocomposites, samples with different INT-WS_2 content were examined. Figure 1 shows the DSC melting thermograms for neat PLLA and PLLA/INT-WS_2 nanocomposites recorded at heating rates of 1, 2, 5, 10 and 20 °C/min after rapid cooling from 225 °C at 40 °C/min, and the specific values of the crystalline parameters of all samples are listed in Table 1.

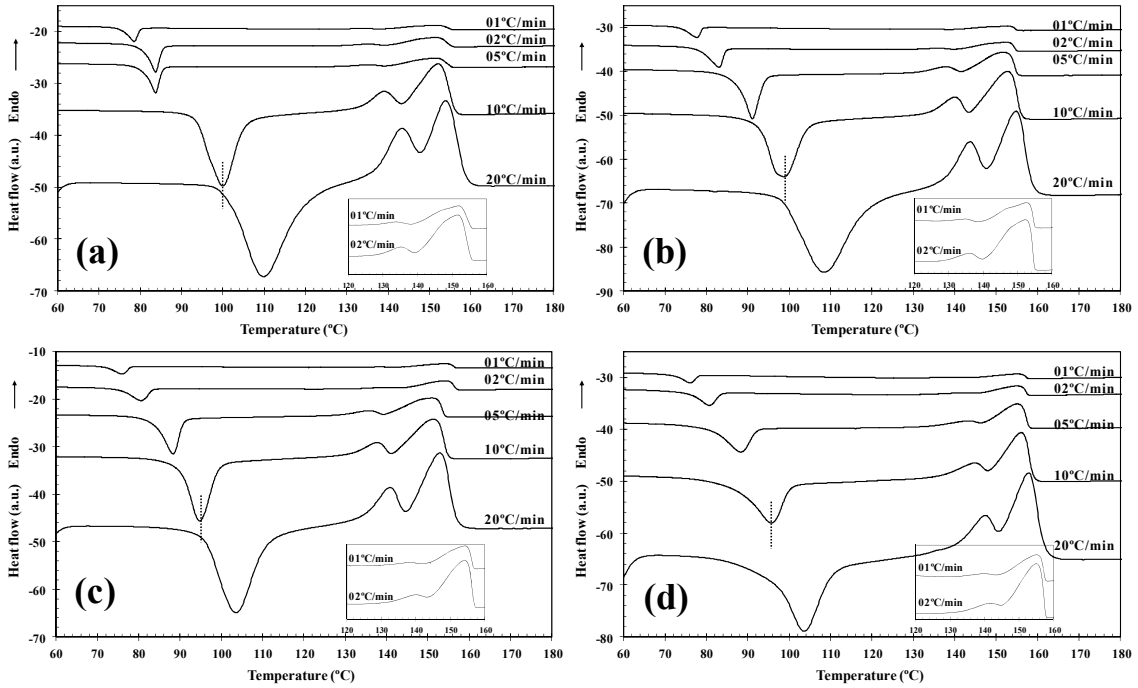

Figure 1. DSC melting thermograms of (**a**) PLLA; and PLLA/INT-WS_2 nanocomposites of (**b**) 0.1; (**c**) 0.5; and (**d**) 1.0 wt % of INT-WS_2 recorded at indicated heating rates after rapid cooling at 40 °C/min.

Table 1. Cold-crystallization and melting parameters for pure poly(L-lactic acid) (PLLA) and PLLA/inorganic nanotubes (INT-WS_2) nanocomposites.

INT-WS_2 content (wt %)	ϕ_h (°C/min)	T_{cc} (°C)	$(1-\lambda)_{cc}$ (%)	T_{m1} (°C)	T_{m2} (°C)	$(1-\lambda)_m$ (%)
0.0	1	78.5	33.7	133.8	152.0	38.9
	2	83.7	37.7	135.3	151.6	41.1
	5	91.5	44.5	137.1	151.3	45.3
	10	99.9	45.7	139.1	152.1	46.8
	20	109.8	45.4	143.4	153.9	46.1
0.1	1	77.6	32.2	134.9	152.9	39.7
	2	83.0	34.4	136.0	152.3	40.8
	5	91.1	42.9	137.8	151.6	46.2
	10	98.6	44.8	140.0	152.7	47.1
	20	108.4	44.6	143.6	154.8	46.4
0.5	1	75.9	28.1	138.5	154.2	40.8
	2	80.5	32.4	139.8	154.2	42.7
	5	88.3	40.6	135.8	151.0	47.0
	10	94.7	42.6	137.8	151.3	47.9
	20	103.5	44.4	140.9	153.0	47.5
1.0	1	76.0	25.0	140.4	155.1	43.0
	2	80.7	30.5	141.6	155.0	46.1
	5	88.2	33.1	143.2	155.1	48.2
	10	95.6	40.5	145.0	156.0	49.7
	20	103.6	43.0	147.4	157.8	45.5

During heating, the exothermic peaks attributed to the cold-crystallization process appear for the samples crystallized at higher cooling rates, indicating that the melt-crystallization process during the prior cooling step was incomplete. The double melting peak was widely observed and will be discussed later. Both heating rate and INT-WS_2 loading were the two main factors that affected the non-isothermal cold-crystallization behaviour of PLLA in the nanocomposites. With increasing heating rate, the crystallization exotherms became broader, and the cold-crystallization peak temperature (T_{cc}) shifted to higher temperature. Moreover, at a given heating rate (for example, 10 °C/min), T_{cc} for neat PLLA was 99.9 °C, whereas T_{cc} for 0.1, 0.5 and 1.0 wt % were found to be 98.6, 94.7, and 95.6 °C, respectively. In particular, at a concentration of 0.5 wt % of INT-WS_2 the value of T_{cc} for PLLA continued to decrease and tended to stabilize, or to slightly increase, for the highest concentration of 1.0 wt %, Table 1. This evolution of the nucleation effect with the concentration of INTs could be related to the variation of the level of the dispersion of the INTs with increasing INT-WS_2 content. The T_{cc} values of neat PLLA and its nanocomposites at various heating rates were plotted in Figure 2. It is clear from Figure 2a that T_{cc} shifted towards higher temperatures with increasing heating rate for all the samples. Moreover, the values of T_{cc} also apparently decreased with increasing INT-WS_2 content, relative to neat PLLA, at all heating rates (Figure 2b). Such results indicate that the incorporation of INT-WS_2 significantly enhanced the non-isothermal cold-crystallization of PLLA matrix, to a degree that was strongly dependent on the INT-WS_2 content. Further, the crystallinity value $(1-\lambda)_{cc}$ calculated for PLLA/INT-WS_2 samples (Figure 3) was affected not only by the heating rate but also by the INT-WS_2 loading, increasing with increasing heating rate (Figure 3a), being more pronounced in the case of the nanocomposites. That is to say, whereas the crystallinity of PLLA was lower at slower heating rate (33.7% at 1 °C/min) and became increasingly higher as the heating rate was increased (45.4% at 20 °C/min), in the case of the nanocomposites with 1.0 wt % of INT-WS_2, the increment in crystallinity observed varied from 25% to 43% at the same heating rates. The influence of INT-WS_2 content on the crystallinity of PLLA is illustrated in Figure 3b, where the $(1-\lambda)_{cc}$ values are represented at different INT-WS_2 loadings. Similar to the results shown in Figure 2b, the presence of INT-WS_2 induces a remarkable decrease in the crystallinity of PLLA in the nanocomposites with respect to neat PLLA at a relatively slow heating rate of 1 °C/min, becoming smaller as the heating rate was increased. This is probably due to the presence of a higher percentage of crystals formed during cooling that reduce the chain mobility. This reduction negatively affects the cold-crystallization process. The remarkable decrease in the crystallinity and T_{cc} of PLLA obtained at low inorganic nanotubes loadings ($\leqslant$0.5 wt %) indicates that INT-WS_2 act as efficient nucleating agents in the PLLA matrix under non-isothermal conditions.

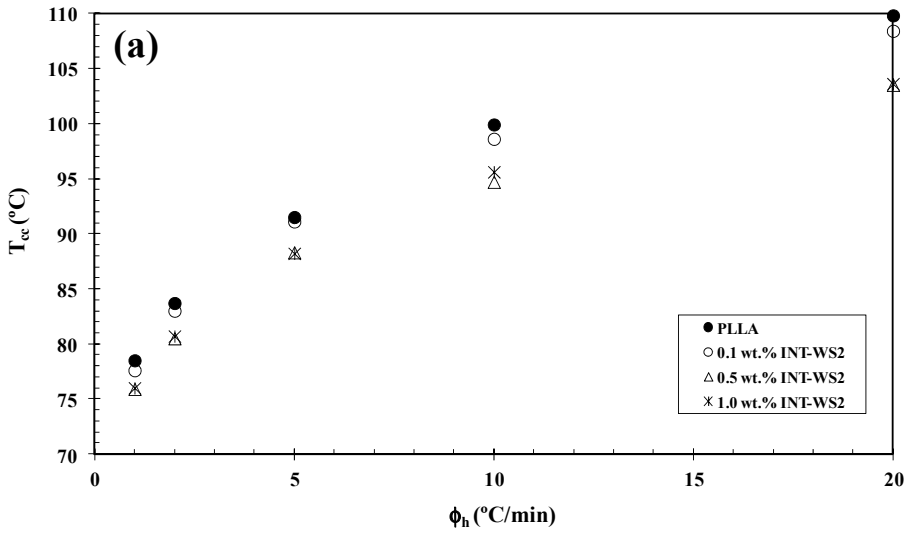

Figure 2. *Cont.*

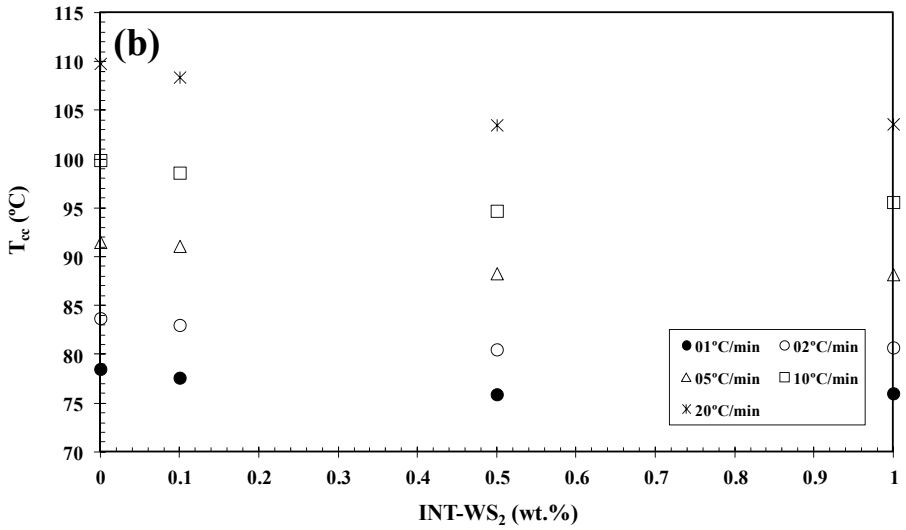

Figure 2. Variation of the cold-crystallization peak temperature (T_{cc}) of PLLA/INT-WS_2 nanocomposites with (**a**) heating rate and (**b**) INT-WS_2 concentration.

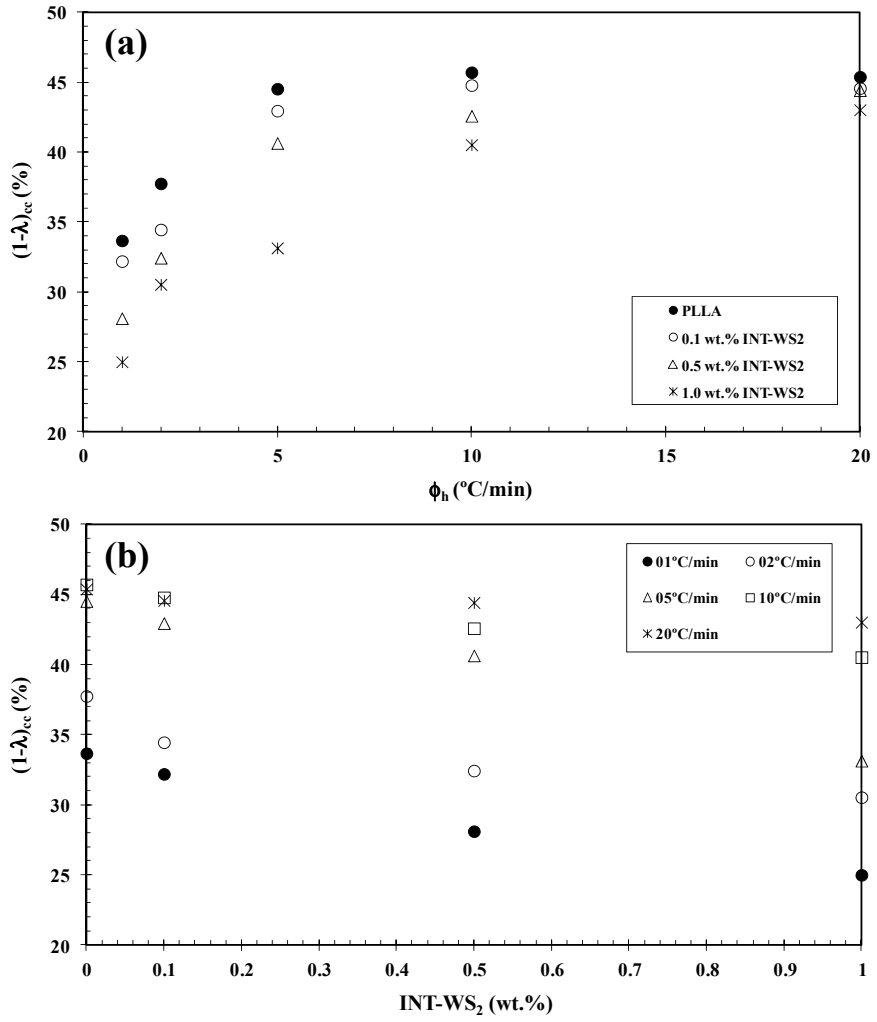

Figure 3. Variation of the cold-crystallinity $(1-\lambda)_{cc}$ of PLLA/INT-WS_2 nanocomposites with **(a)** heating rate and **(b)** INT-WS_2 concentration.

In the case of polymer crystallization, the measured rate of heat release is assumed to be proportional to the macroscopic rate of crystallization:

$$\frac{dQ}{dt} = Q_c \frac{dx}{dt} \tag{2}$$

where Q_c is the measured heat of crystallization calculated by integration of a DSC peak. The values of Q_c can further be used to determine the crystallization rate, dx/dt, as well as the extent of the melt conversion:

$$x(t) = \frac{1}{Q_c} \int_0^t \frac{dQ}{dt} dt \tag{3}$$

The value of $x(t)$ varies from 0 to 1 and represents the degree of conversion. The transformation from temperature to time is performed using a constant heating rate ϕ:

$$t = \frac{T_0 - T}{\phi} \tag{4}$$

where T is the temperature at time t and T_i is the temperature at the beginning of crystallization. Figure 4 shows typical conversion curves at various heating rates for PLLA/INT-WS_2 nanocomposites. The conversion curves shift over a longer time with decreasing heating rate, suggesting that the diffusion of PLLA becomes very difficult for cold-crystallization.

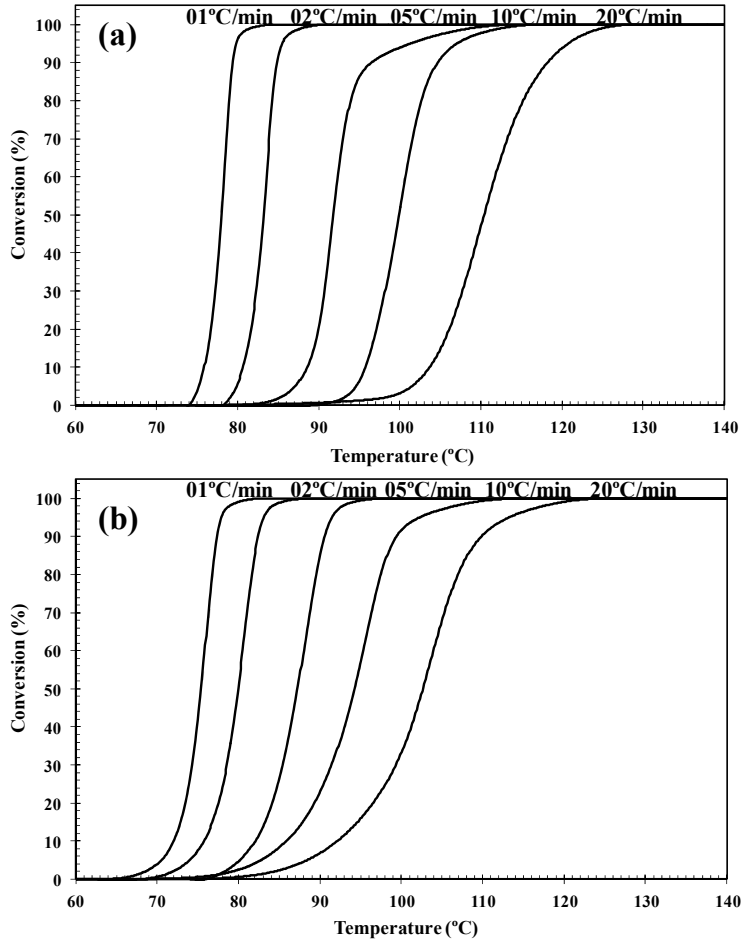

Figure 4. Conversion curves for the cold-crystallization of **(a)** PLLA and **(b)** PLLA/INT-WS_2 (1.0 wt %).

3.2. Lui Model

To quantitatively describe the evolution of crystallinity during non-isothermal crystallization, a number of models have been proposed in the literature [30]. The most common approach is that proposed by Lui *et al.* [31] who combined the Avrami and Ozawa models [32–35] to analyze the non-isothermal crystallization kinetics. Since the degree of crystallinity is related to the heating rate (ϕ) and the crystallization time t, or temperature T, and the relation between ϕ and t can be established for a particular degree of crystallinity, the final expression of their model can be written as follows:

$$ln\phi = lnf\,(T) - \alpha lnt \tag{5}$$

where $f(T)$ = [k´(T)/k]$1/m$, corresponds to the value of heating rate chosen at unit crystallization time, when the system has a certain degree of crystallinity, α is the ratio of the Avrami exponents to Ozawa exponents (*i.e.*, $\alpha = n/m$), and ϕ is the heating rate. Plotting $ln\ \phi$ *vs.* ln t at a given degree of conversion yields a linear representation, as shown in Figure 5. This indicates that the Lui model provides a satisfactory description for the cold-crystallization of PLLA/INT-WS_2 nanocomposites. The kinetic parameters, ln *f(T)* and α, which are derived from the slope and the intercept of those lines, are listed in Table 2. These data show that *f(T)* for PLLA increases rapidly with the crystallinity from 83.58 for x = 10% to 114.42 for x = 90%. Noticeably, *f(T)* for PLLA is much greater than that for PLLA/INT-WS_2 for the same conversion x and the effect becomes less pronounced with increasing nanoparticle loading ($\geqslant$0.5 wt %). This means that to approach an identical degree of crystallinity, the nanocomposites required a higher crystallization rate than that of the pure PLLA. That is to say, the PLLA/INT-WS_2 nanocomposites crystallize easier than PLLA. In addition, the values of the parameter α are nearly constant (1.2 to 1.3), indicating that the mechanism of nucleation and growth is more or less the same for both PLLA and PLLA/INT-WS_2.

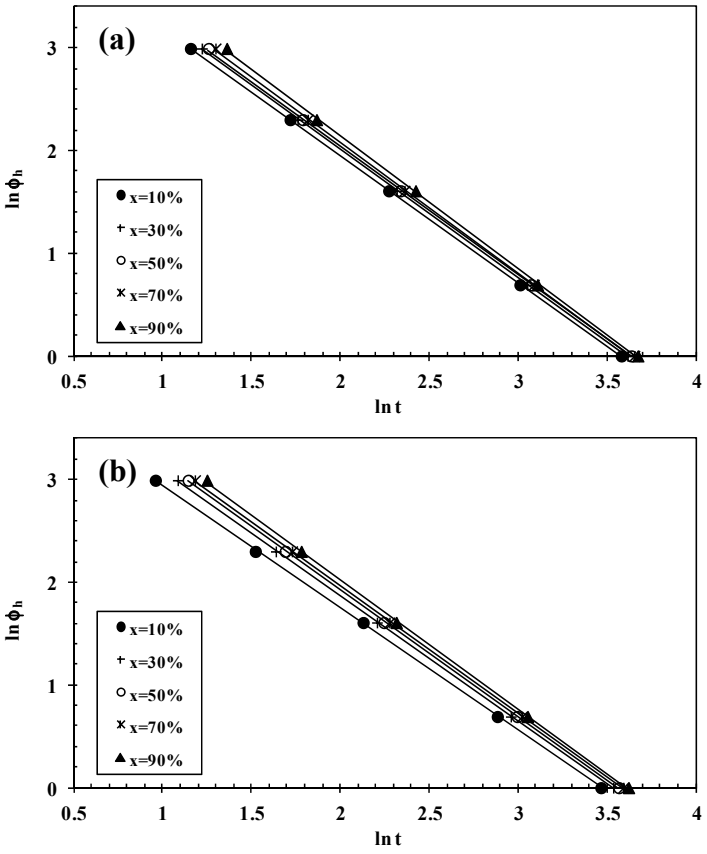

Figure 5. Liu plots for the cold-crystallization of **(a)** PLLA and **(b)** PLLA/INT-WS_2 (1.0 wt %).

Table 2. Values of α and *f(T) vs.* conversion (x) based on the Liu model for pure PLLA and PLLA/INT-WS_2.

INT-WS_2 content (wt %)	x (%)	α	$F(T)$	ΔE^a (kJ/mol)
0.0	10	1.24	83.58	100.8
	30	1.25	90.89	
	50	1.26	95.76	
	70	1.27	101.73	
	90	1.29	114.42	
0.1	10	1.24	80.29	102.7
	30	1.24	87.02	
	50	1.26	93.30	
	70	1.27	99.31	
	90	1.30	111.33	
0.5	10	1.23	73.09	112.8
	30	1.24	79.65	
	50	1.24	83.31	
	70	1.25	87.24	
	90	1.26	95.24	
1.0	10	1.29	62.41	111.9
	30	1.22	74.47	
	50	1.24	81.18	
	70	1.24	85.88	
	90	1.26	95.10	

3.3. Effective Energy Barrier

Activation energy is an important parameter for characterizing the non-isothermal crystallization of polymers and can be used to estimate the growth ability of the chain segments. The higher the crystallization activation energy ΔE, the more difficult is the transport of macromolecular segments to the growing surface. Considering the variation of the peak temperature with the heating rate ϕ, ΔE could be derived from the Kissinger equation [36]:

$$ln\left(\frac{\phi}{T_{cc}^2}\right) = Constant - \frac{\Delta E}{RT_{cc}} \quad (6)$$

where R is the universal gas constant. The activation energies were calculated using the slopes of the lines obtained from plots of log $\phi/{T_{cc}}^2$ against $1/T_{cc}$ (Figure 6). Thus the values of ΔE for neat PLLA and its nanocomposite containing 0.1 wt % of INT-WS_2 were calculated to be 100.8 and 102.7 kJ/mol, respectively (Table 2). At higher INT-WS_2 concentrations, the value of ΔE for PLLA continues to rise and tends to stabilize for the highest concentrations of 0.5% and 1% (*i.e.*, $\Delta E_{0.5}$ = 112.8 kJ/mol and $\Delta E_{1.0}$ = 111.9 kJ/mol.

It was also noticed that the primary crystallization is an interface-controlled process with a decreasing nucleation rate. Thus, it is evident that the crystallization process is complex (and not isokinetic) during the entire crystallization event. The complexity of the crystallization mechanism can be judged from the dependence of ΔE on crystalline conversion using the so-called differential isoconversional method of Friedman [37], according to the following expression:

$$ln\left(\frac{dx}{dt}\right)_{x,i} = Constant - \frac{\Delta E_x}{RT_{x,i}} \quad (7)$$

where dx/dt is the instantaneous crystallization rate as a function of time at a given conversion x. By selecting the appropriate conversion (*i.e.*, from 10% to 90%) the values of dx/dt at a specific x are correlated to the corresponding crystallization temperature at this x (*i.e.*, T_x). Then, from the slopes of these representations for the PLLA and the nanocomposites, the ΔE can be calculated. As an example,

Figure 7 shows the dependence of the effective energy barrier on conversion x for neat PLLA and its nanocomposites with 0.1, 0.5 and 1.0 wt % of INT-WS_2. As can be seen, the effective energy barrier decreases as the conversion rises and the temperature increases. Thus, isoconversional methods not only provide accurate value of activation energy, but it also hints towards the degree of complexity of the crystallization mechanism from the knowledge of the dependence of ΔE on x. According to this Figure, at a given x, the effective energy barrier is dependent on the INT-WS_2 concentration. More importantly, the apparent ΔE values of the all nanocomposites are higher than that of neat PLLA, indicating that the restriction of molecular mobility of PLLA chains does not appear to be a limiting factor in the crystallization rate, and demonstrating that the nucleation activity of INTs plays a dominant role in accelerating the crystallization of PLLA.

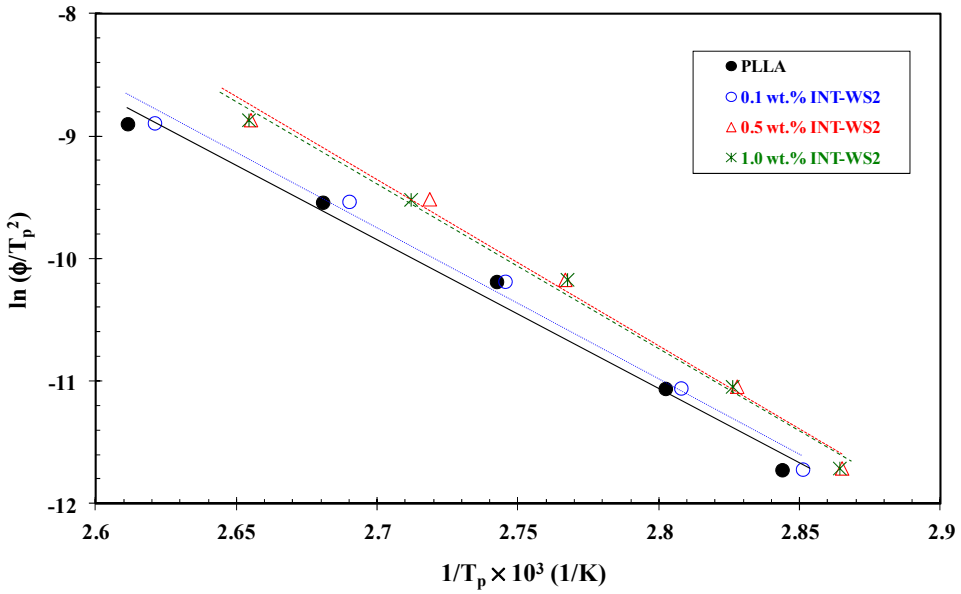

Figure 6. Kissinger plots for the cold-crystallization of PLLA/INT-WS_2 nanocomposites.

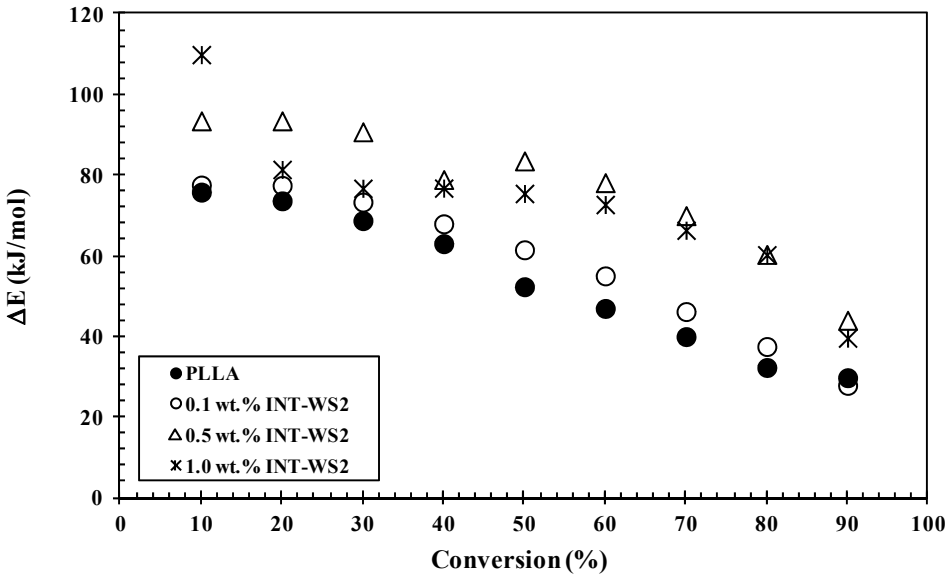

Figure 7. Dependence of the effective energy barrier (ΔE) on the degree of conversion (x) of PLLA/INT-WS_2 nanocomposites using differential isoconversional methods of Friedman.

3.4. Melting Behaviour

It is of interest to evaluate the effect of heating rate on the melting behaviour of PLLA in the nanocomposites. As shown in Figure 1, the heating rate effect is evident in all samples, which led to the appearance of complex double-melting peaks. The first peak was observed at 134–143 °C and the other at 152–154 °C (Table 1). The analogous data of double-melting peaks *versus* heating rate with INT-WS_2 concentration as a parameter are also shown in Table 1. In general, it is accepted that the double endothermic peaks are attributed to melting-recrystallization-melting processes of PLLA lamellae. Obviously, the first endothermic peak is attributed to the fusion of thin lamellae formed during the DSC heating process (e.g., cold-crystallization), and the second to the fusion of lamellae that are newly formed through the melting-recrystallization of primary thin lamellae occurring at relatively higher temperature [38,39]. In particular, an increasing heating rate allows less time for the crystals to reorganize and re-melting occurs over a lower temperature range. Ideally, the melting of reorganized crystals should completely vanish over a certain heating rate where recrystallization is totally inhibited. Therefore, the first endothermic peak can be used to reflect the lamellar structure of PLLA in the nanocomposites. Figure 8a compares the evolution of melting temperatures for pure PLLA and PLLA/INT-WS_2 as a function of the cooling rate. The low and high-temperature melting endotherms were labelled T_{m1} and T_{m2}, respectively. T_{m1} gradually shifted to higher temperature with increasing heating rate, whereas T_{m2} showed much lower dependence on the heating rate. On the other hand, increasing amounts of INT-WS_2 in the PLLA/INT-WS_2 nanocomposites progressively reduces the apparent area under the first endotherm. These results confirm that the double-melting behaviour of the samples is mainly derived from the melting-recrystallization-remelting processes upon heating. However, the most relevant result was the reduction of the difference between the melting temperature peaks of the nanocomposite and that of the neat matrix (T_{m2}–T_{m1}) with increasing heating rate. This phenomenon was less pronounced for the nanocomposites with high INT-WS_2 contents, which also exhibited lower recrystallization at a given heating rate (Figure 8b). Therefore, the crystals in the nanocomposites are more perfect and stable than those in neat PLLA. This is related to the strong nucleation effect of INT-WS_2 involved in the acceleration of the crystallization of PLLA in the nanocomposites and is also in agreement with the aforementioned shift of the crystallization ranges of PLLA along the crystallization temperature axis.

In tune with these observations, both heating rate and (the INT-WS_2 loading are the two main factors that influence the crystallinity of PLLA in the nanocomposites Table 1). On the one hand, with increasing heating rate, $(1\text{-}\lambda)_m$ shifts towards higher values, and the melting process is enhanced for both neat PLLA and its nanocomposites. On the other hand, the addition of INT-WS_2 apparently enhances $(1\text{-}\lambda)_m$ of PLLA when a low cooling rate is used. For more clarity, Figure 9 summarizes the variation of $(1\text{-}\lambda)_m$ with heating rate and composition. The data presented also shows the difference between the overall crystallinity change derived from the difference between endotherm and exotherm, $\Delta(1\text{-}\lambda) = (1\text{-}\lambda)_m - (1\text{-}\lambda)_{cc}$, for neat PLLA and its nanocomposites, which can be used to highlight the recrystallization ability of the PLLA crystals. At lower $\Delta(1\text{-}\lambda)$, the reorganization of the PLLA crystals is more difficult. It can be seen that increasing the heating rate allows less time for the molten materials to reorganize into new crystals, thus lowering $\Delta(1\text{-}\lambda)$ (Figure 9a) and hence, the reorganization process is largely inhibited. On the other hand, the INT-WS_2 have shown an important capacity for accelerating the cold-crystallization process (discussed earlier) and reducing the crystallinity $(1\text{-}\lambda)_{cc}$ due to a remarkable heterogeneous nucleation role in the nanocomposites. However, the role of INT-WS_2 on the variation of the $\Delta(1\text{-}\lambda)$ values of PLLA appears to be only relevant at a low heating rate. These results confirm that the variation of $\Delta(1\text{-}\lambda)$ is mainly derived from the melting-recrystallization-remelting processes upon heating. However, in our case, we cannot exclude the nucleation capacity of INT-WS_2 during cooling, which may induce the generation of new crystals of PLLA in the nanocomposites. That is, the difference $\Delta(1\text{-}\lambda)$ may involve both nucleation during cooling as well as reorganization ability of the PLLA crystals during subsequent heating.

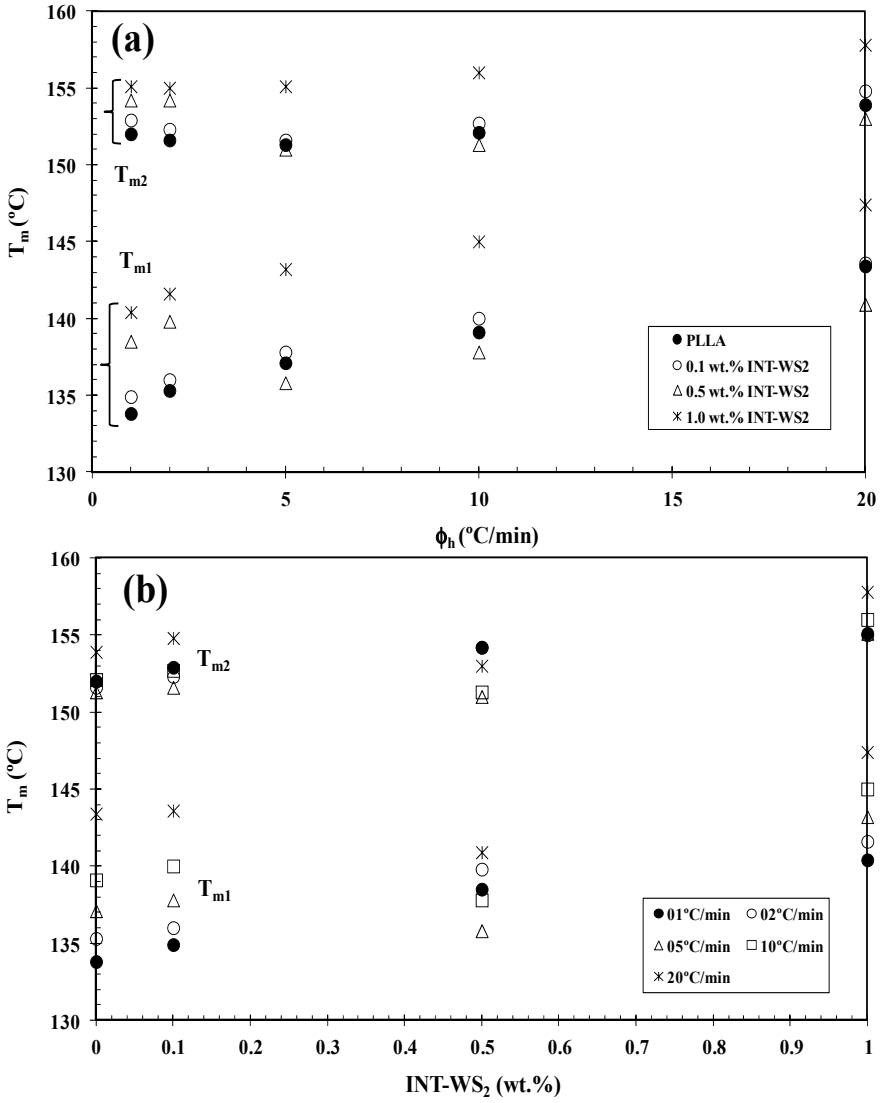

Figure 8. Variation of the melting temperatures (T_{m1} and T_{m2}) of PLLA/INT-WS_2 nanocomposites with **(a)** heating rate and **(b)** INT-WS_2 concentration.

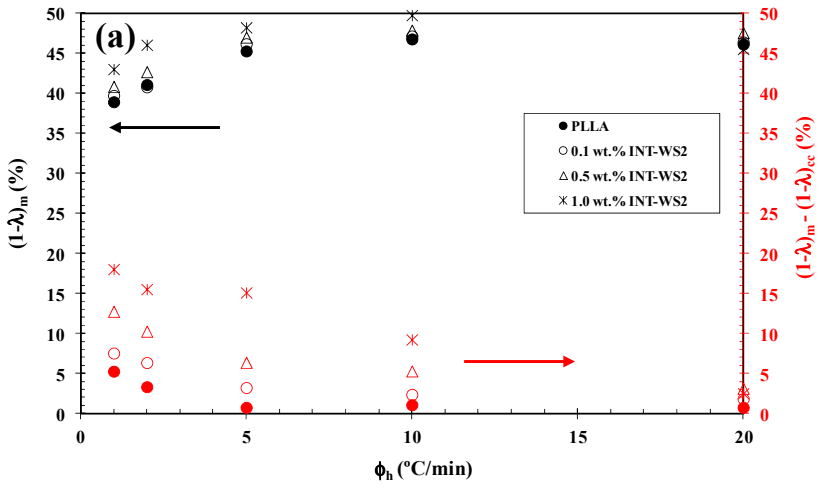

Figure 9. *Cont.*

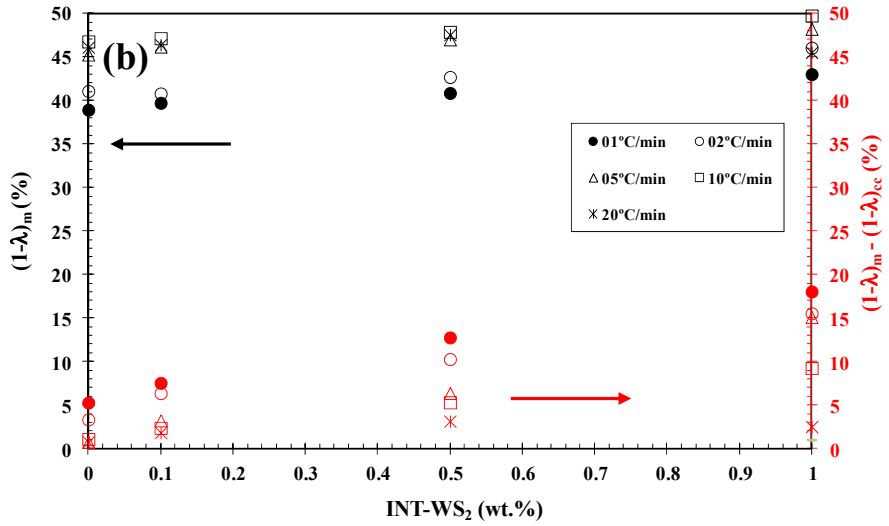

Figure 9. Variation of the melting crystallinity $(1-\lambda)_m$ of PLLA/INT-WS_2 nanocomposites with **(a)** heating rate and **(b)** INT-WS_2 concentration; inset is the difference between the overall crystallinity change derived from the difference between endotherm and exotherm, $\Delta(1-\lambda)=(1-\lambda)_m-(1-\lambda)_{cc}$, for PLLA/INT-$WS_2$ nanocomposites.

4. Conclusions

The results of our study demonstrate the effectiveness of the use of small amounts of INT-WS_2 to improve the cold-crystallizability of PLLA biopolymer. The results obtained from the DSC analysis show that the heating rate and INT-WS_2 loading are very efficient factors for the control of the cold-crystallization rate and crystallinity of PLLA. In particular, it was shown that INT-WS_2 enhanced the crystallization rate of PLLA significantly, and the degree of enhancement is strongly dependent on the INT-WS_2 content. The introduction of INT-WS_2 to the PLLA matrix induces a remarkable decrease in the $(1-\lambda)_{cc}$ value of PLLA at a relatively slow heating rate of 1 °C/min, becoming smaller as the heating rate was increased. The Lui model was found to be effective in describing the crystallization of PLLA/INT-WS_2 nanocomposites. All rate parameters demonstrated that the PLLA/INT-WS_2 crystallized easier than pure PLLA due to excellent nucleating effect of INT-WS_2. Further, the energy barrier governing the crystallization, calculated based on isokinetic and differential (Friedman) isoconversional methods, confirmed that the nucleation activity of INTs plays a dominant role in accelerating the crystallization of PLLA. However, the nucleation mechanism of PLLA remains unchanged. On subsequent heating, double-melting peaks for PLLA and its nanocomposites can be attributed to a melt-recrystallization mechanism. It was found that increasing the heating rates reduced the difference between the melting temperature peaks of PLLA/INT-WS_2 and that of the neat PLLA (*i.e.*, impeded the recrystallization of PLLA in the nanocomposites). This phenomenon was less pronounced for the nanocomposites with high INT-WS_2 content. In addition, the difference in the apparent crystallinity $\Delta(1-\lambda)$ was found to be an effective method to highlight the recrystallization ability of the PLLA crystals. The quantitative analysis showed that increasing the heating rate can effectively inhibit the reorganization process of PLLA, and a further increase of the INT-WS_2 concentration led to a marked influence on the recrystallization of PLLA, especially when at low heating rates. These results have considerable practical significance for technological processing of PLLA, where premature crystallization hinders the forming stage, and offers new prospects for the preparation of PLLA biopolymer materials for possible use in many eco-friendly (e.g., sustainable packaging) and biomedical (e.g., surgical sutures, bone fixation devices, *etc.*) applications.

Acknowledgments: This work was supported by the Spanish Ministry Economy and Competitivity (MINECO), Projects MAT-2010-21070-C02-01 and MAT2013-41021-P. Mohammed Naffakh would also like to acknowledge the MINECO for a "Ramón y Cajal" Senior Research Fellowship. Very special thanks and appreciation go to Alla Zak for providing the WS_2 inorganic nanotubes.

Author Contributions: Mohammed Naffakh conceived and designed the work, and prepared and characterized the materials; Carlos Marco performed the DSC experiments and analyzed the theoretical kinetic models. All authors contributed to the discussion and writing of the manuscript.

Conflicts of Interest: The authors declare no conflict of interest.

References

1. Ikada, Y.; Tsuji, H. Biodegradable polyesters for medical and ecological applications. *Macromol. Rapid Commun.* **2000**, *21*, 117–132.
2. Sodergard, A.; Stolt, M. Properties of lactic acid based polymers and their correlation with composition. *Prog. Polym. Sci.* **2002**, *27*, 1123–1163. [CrossRef]
3. Rasal, R.M.; Janrkor, A.V.; Hirt, D.E. Poly(lactic acid) modifications. *Prog. Polym. Sci.* **2010**, *35*, 338–356. [CrossRef]
4. Lim, L.T.; Auras, R.; Rubino, M. Processing technologies for poly(lactic acid). *Prog. Polym. Sci.* **2008**, *33*, 820–882. [CrossRef]
5. Othman, N.; Acosta-Ramírez, A.; Mehrkhodavandi, P.; Dorgan, J.R.S.; Hatzikiriakos, G. Solution and melt viscoelastic properties of controlled microstructure poly(lactide). *J. Rheol.* **2011**, *55*, 987–1005. [CrossRef]
6. Othman, N.; Xu, C.; Mehrkhodavandi, P.; Hatzikiriakos, S.G. Thermorheological and mechanical behavior of polylactide and its enantiomeric diblock copolymers and blends. *Polymer* **2012**, *53*, 2443–2452. [CrossRef]
7. Saeidou, S.; Huneault, M.A.; Li, H.; Park, C.B. Poly(lactic acid) crystallization. *Prog. Polym. Sci.* **2012**, *37*, 1657–1677. [CrossRef]
8. Naffakh, M.; Díez-Pascual, A.M.; Marco, C.; Ellis, G.; Gómez-Fatou, M.A. Opportunities and challenges in the use of inorganic fullerene-like nanoparticles to produce advanced polymer nanocomposites. *Prog. Polym. Sci.* **2013**, *38*, 1163–1231. [CrossRef]
9. Naffakh, M.; Díez-Pascual, A.M. Thermoplastic polymer nanocomposites based on inorganic fullerene-like nanoparticles and inorganic nanotubes. *Inorganics* **2014**, *2*, 291–312. [CrossRef]
10. Tenne, R.; Margulis, L.; Genut, M.; Hodes, G. Polyhedral and cylindrical structures of tungsten disulphide. *Nature* **1992**, *360*, 444–445. [CrossRef]
11. Margulis, L.; Salitra, G.; Tenne, R.; Talianker, M. Nested fullerene-like structures. *Nature* **1993**, *365*, 113–114. [CrossRef]
12. Rao, C.N.R.; Nath, M. Inorganic nanotubes. *Dalton Trans.* **2003**, 1–24. [CrossRef]
13. Remškar, M. Inorganic nanotubes. *Adv. Mater.* **2004**, *16*, 1497–1504. [CrossRef]
14. Tenne, R. Inorganic nanotubes and fullerene-like nanoparticles. *Nat. Nanotechnol.* **2006**, *1*, 103–111. [CrossRef] [PubMed]
15. Tenne, R.; Redlich, M. Recent progress in the research of inorganic fullerene-like nanoparticles and inorganic nanotubes. *Chem. Soc. Rev.* **2001**, *39*, 1423–1434. [CrossRef] [PubMed]
16. Zak, A.; Sallacan-Ecker, L.; Margolin, A.; Genut, M.; Tenne, R. Insight into the growth mechanism of WS_2 nanotubes in the scaled-up fluidized-bed reactor. *Nano* **2009**, *4*, 91–98. [CrossRef]
17. Zak, A.; Sallacan Ecker, L.; Fleischer, N.; Tenne, R. Large-scale synthesis of WS_2 multiwall nanotubes and their dispersion, an update. *Sens. Transducers. J.* **2011**, *12*, 1–10.
18. Zhu, Y.Q.; Sekine, T.; Brigatti, K.S.; Firth, S.; Tenne, R.; Rosentsveig, R.; Kroto, H.W.; Walton, D.R. Shock-wave resistance of WS_2 nanotubes. *J. Am. Chem. Soc.* **2003**, *125*, 1329–1333. [CrossRef] [PubMed]
19. Komarneni, M.; Sand, A.; Nevin, P.; Zak, A.; Burghaus, U. Absorption and reaction kinetics of small organic molecules on WS_2 nanotubes: An ultra-high vacuum study. *Chem. Phys. Lett.* **2009**, *479*, 109–112. [CrossRef]
20. Pardo, M.; Shuster-Meiseles, T.; Levin-Zaidman, S.; Rudich, A.; Rudich, Y. Low cytotoxicity of inorganic nanotubes and fullerene-like nanostructures in human bronchial epithelial cells: Relation to inflammatory gene induction and antioxidant response. *Environ. Sci. Technol.* **2014**, *48*, 3457–3466. [CrossRef] [PubMed]
21. Goldman, E.B.; Zak, A.; Tenne, R.; Kartvelishvily, E.; Levin-Zaidman, S.; Neumann, Y.; Stiubea-Cohen, R.; Palmon, A.; Hovav, A.H.; Aframian, D.J. Biocompatibility of tungsten disulfide inorganic nanotubes and

fullerene-like nanoparticles with salivary gland cells. *Tissue Eng. Part A* **2015**, *21*, 1013–1023. [CrossRef] [PubMed]
22. Reddy, C.S.; Zak, A.; Zussman, E. WS_2 nanotubes embedded in PMMA nanofibers as energy absorptive material. *J. Mater. Chem.* **2001**, *21*, 16086–16093. [CrossRef]
23. Lalwani, G.; Henslee, A.M.; Farshid, B.; Parmar, P.; Lin, L.; Qin, Y.X.; Kasper, F.K.; Mikos, A.G.; Sitharaman, B. Tungsten disulfide nanotubes reinforced biodegradable polymers for bone tissue engineering. *Acta Biomater.* **2013**, *9*, 8365–8373. [CrossRef] [PubMed]
24. Naffakh, M.; Marco, C.; Ellis, G. Inorganic WS_2 nanotubes that improve the crystallization behavior of poly(3-hydroxybutyrate). *CrystEngComm* **2014**, *16*, 1126–1135. [CrossRef]
25. Naffakh, M.; Díez-Pascual, A.M. Nanocomposite biomaterials based on poly(etherether-ketone) (PEEK) and WS_2 inorganic nanotubes. *J. Mater. Chem. B* **2014**, *2*, 4509–4520. [CrossRef]
26. Naffakh, M.; Marco, C.; Ellis, G. Development of novel melt-processable biopolymer nanocomposites based on poly(L-lactic acid) and WS_2 inorganic nanotubes. *CrystEngComm* **2013**, *16*, 5062–5072. [CrossRef]
27. Fischer, E.W.; Sterzel, H.J.; Wegner, G. Investigation of the structure of solution grown crystals of lactide copolymers by means of chemical reactions. *Kolloid Z. Z. Polym.* **1973**, *251*, 980–990. [CrossRef]
28. Hoffman, J.D.; Miller, R.L. Kinetics of crystallization from the melt and chain folding in polyethylene fractions revisited: theory and experiment. *Polymer* **1997**, *38*, 3151–3212. [CrossRef]
29. Ferry, J.D. *Viscoelastic Property of Polymers*, 2nd ed; Wiley: New York, NY, USA, 1970.
30. Di Lorenzo, M.L.; Silvestre, C. Non-isothermal crystallization of polymers. *Prog. Polym. Sci.* **1999**, *24*, 917–950. [CrossRef]
31. Liu, T.; Mo, Z.; Wang, S.; Zhang, H. Nonisothermal melt and cold crystallization kinetics of poly(aryl ether ether ketone ketone). *Polym. Eng. Sci.* **1997**, *37*, 568–575. [CrossRef]
32. Avrami, M. Kinetics of phase changes. I General theory. *J. Chem. Phys.* **1939**, *7*, 1103–1112. [CrossRef]
33. Avrami, M. Kinetics of phase change. II Transformation-time relations for random distribution of nuclei. *J. Chem. Phys.* **1940**, *8*, 212–224. [CrossRef]
34. Avrami, M. Kinetics of phase change. III Granulation, phase change, and microstructure. *J. Chem. Phys.* **1941**, *9*, 177–184. [CrossRef]
35. Ozawa, T. Kinetics of non-isothermal crystallization. *Polymer* **1971**, *128*, 150–158. [CrossRef]
36. Kissinger, H.E. Variation of peak temperature with heating rate in differential thermal analysis. *J. Res. Natl. Bur. Stand.* **1956**, *57*, 217–221. [CrossRef]
37. Fridman, H. Kinetics of thermal degradation of char-forming plastics from thermogravimetry. Application to a phenolic plastic. *J. Polym. Sci. Part C* **1964**, *6*, 183–195. [CrossRef]
38. He, Y.; Fan, Z.Y.; Wei, J.; Li, S.M. Morphology and melt crystallization of poly(L-lactide) obtained by ring opening polymerization of L-lactide with zinc catalyst. *Polym. Eng. Sci.* **2006**, *46*, 1583–1589. [CrossRef]
39. Chen, H.C.; Chen, J.; Shao, L.; Yang, J.H.; Huang, T.; Zhang, N.; Wang, Y. Comparative study of poly(L-lactide) nanocomposites with organic montmorillonite and carbon nanotubes. *J. Polym. Sci. Polym. Phys.* **2013**, *51*, 183–196. [CrossRef]